Hindawi
Geofluids
Volume 2021, Article ID 9920415, 12 pages
https://doi.org/10.1155/2021/9920415

Research Article

The Promotion/Inhibition of the Seepage Transport of Copper Ions by Suspension-Colloidal Particles with Wide Size Gradation

Qingke Nie,[1,2] **Huawei Li**,[1,2] **Haipeng Yang**,[2] **Tengfei Ni**,[3] **and Sichen Jiang**[3]

[1]*Hebei Research Institute of Construction and Geotechnical Investigation Co., Shijiazhuang 050031, China*
[2]*Geotechnical Engineering Research Center of Hebei Province, Shijiazhuang 050031, China*
[3]*Key Laboratory of Urban Underground Engineering of Ministry of Education, Beijing Jiaotong University, Beijing 100044, China*

Correspondence should be addressed to Qingke Nie; niealex@126.com

Received 4 March 2021; Accepted 20 May 2021; Published 30 May 2021

Academic Editor: Mercè Corbella

Sand column tests were conducted to investigate the seepage transport of silicon powders (SPs) with two wide particle size ranges (30-2000 nm and 2-70 μm), including the cotransport of SPs and copper ions. The results show that the graded large-scale SP has an obvious inhibiting influence on the transport of copper ions. In contrast, in the presence of the graded small-scale SP, the concentration of copper ions in the effluent tends to increase; i.e., there appears to be a promoting effect. However, after a long transport distance, the presence of SPs, regardless of particle size, has an overall retarding effect on heavy metal pollutants (e.g., copper ions). The promoting effect of the increase in seepage velocity on the concentration of copper ions in the effluent is greater with the graded large-scale SPs than with the graded small-scale SPs. In terms of the microstructural characteristics by metallographic microscopy, the average particle size of the deposited graded small-scale SPs is almost constant at different transport distances, while that of the deposited graded large-scale SPs tend to decrease significantly with increasing transport distance; i.e., notable bed filtration is exhibited in the latter case. This physical mechanism also determines the sequence and rate of the retarding effect of SPs on heavy metal ions under seepage flow.

1. Introduction

The transport processes, retardation mechanisms, and control measures of heavy metal pollutants in permeable soils remain an important topic [1, 2] in the fields of environmental geotechnical engineering, ocean engineering, hydrology, engineering geology, municipal engineering, and even agricultural sciences [3], covering the seepage control of municipal solid waste landfills and industrial tailings ponds [4–6], treatment of contaminated groundwater [7–9], mining processes of metallic minerals [10, 11], environmental damage caused by the use of pesticides and fertilizers [12], and treatment of municipal wastewater [13, 14]. The movement of heavy metal pollutants and tiny suspended particles in soils is a complex process, in which the two either promote or inhibit each other. The final effect is determined by the influence of numerous physicochemical factors [15–18] and is related to the method for evaluating the transport distance. Thus far, many researchers have studied the influences of different types of suspended matters (e.g., montmorillonite colloid, humic acid, and silicon powder (SP)) on the seepage migration of Pb and Cd, concluding that suspended particles can promote the transport of these heavy metal ions under certain conditions [19, 20], with specific occurrence conditions given in some literature [21, 22]. Bai et al. [23] discussed the influence of suspended particles on the migration of lead ions in porous media under pulse injection, showing that the existence of suspended particles promotes the migration of lead ions and that this promoting effect changes significantly with changes in particle size; they attributed this finding to the so-called "size exclusion effect." In fact, the promoting effect of suspended particles gradually diminishes after their size exceeds a certain threshold, and the presence of heavy metal ions inhibits the transport of suspended particles to a certain extent, suggesting a coupling mechanism between the two.

In fact, the factors affecting the coupled transport of suspended particles and heavy metal ions not only include the concentration of suspended particles, particle size [24, 25],

seepage velocity [26, 27], temperature [28, 29], gravity effect [30, 31], and type and pH of heavy metal ions [32] but also include a variety of factors such as the type of porous media and physicochemical properties [33]. In this regard, many laboratory experiments have been accomplished to establish models for the deposition and release of suspended matters [34] as well as to establish the governing equations for the cotransport of multiple components [35–37]. Chrysikopoulos and Katzourakis [38] demonstrated that the dispersivity of colloids is not only a function of colloid size but also a function of seepage velocity by laboratory and field studies. Bedrikovetsky et al. [39] proposed a model for discussing the pore size distribution of porous media from the long-term injection of mono-sized suspension as well as a theoretical model for predicting the corresponding transport process, taking into account the restraining effect of the pore scale of the porous media on the suspended particles as well as the nonlinear characteristics caused by cumulative deposition. Borazjani and Bedrikovetsky [40] derived an analytical solution for two-phase flows with multiple particle-capture mechanisms that can be used to predict the breakthrough profiles and histories of the concentration of retained particles as well as the saturation of each phase in the leachate. Katzourakis and Chrysikopoulos [41] developed analytical solutions for colloid transport in porous media where the colloids can be attached reversibly and/or irreversibly on the matrix. Recently, Bai et al. [42] presented a model with sorption hysteresis, known as the BB model; in this model, they used a family of nonlinear scanning desorption isotherms to describe the detachment mechanism of the deposited suspended matters and introduced a "reaction rate coefficient" to reflect the unsteady flow dynamics of the deposition, release, and transport of suspended particles during seepage.

Due to the size exclusion effect, SPs with small particle sizes are generally believed to promote the seepage transport of heavy metal ions, while those with particle sizes larger than the porous media pore size are captured at the constrictions of narrow pore channels [43, 44]. As mentioned earlier, the cotransport mechanism of heavy metal ions and SP particles depends on their dielectric properties, thereby enhancing the possibility of deposition of SP (together with the heavy metal ions adsorbed thereon). Tang and Weisbrod [45] studied the transport of lead ions in a chalk fracture with an equivalent hydraulic pore diameter; their experimental results showed that lead ions are mobile only when related with tiny particles and that the addition of humic acid not only facilitates the sorption of lead ions on the montmorillonite-humic acid mixture but also improves the recovery of montmorillonite. Sasidharan et al. [46] systematically investigated the coupled effects of hydrodynamic forces and solution chemistry conditions on the long-term deposition kinetics of nanoparticles, concluding that the breakthrough processes of the colloids showed a bimodal pattern with enhancing solution ionic strength. Sun et al. [47] conducted seepage transport experiments with different concentrations of graphene oxide in quartz sand, and they found that the mobility of graphene oxide in sand columns decreases as the grain size decreases, while the retention rate of the particles decreases due to the "blocking" mechanism.

The transport characteristics of suspended particles in multigraded, multiscale porous media have also received research attention. To investigate the effects of pore size distribution on particle size selection and particle recovery, Ikni et al. [48] studied the seepage transport process and the bed filtration of fine sand by using step-input injections; porous media with different pore sizes (i.e., fine medium, coarse medium, or a mixture thereof) were utilized in the experiments, and the results showed that the mixture medium had a wider pore size distribution and therefore a higher particle retention, with the coarser particles being the first to be recovered. In addition, researchers have started to experiment with different suspended particles to remove heavy metal pollutants already deposited in soil to achieve cleaning. Using custom-made laboratory experimental equipment, Bai et al. [49] attempted to employ purifying agents to stimulate the detachment of heavy metal pollutants deposited in quartz sand.

In the present study, one-dimensional sand column tests were conducted to discuss the seepage transport of SPs with two wide particle size ranges (30-2000 nm and 2-70 μm, respectively), including the cotransport of SP and copper ions as well as to investigate influencing factors on the transport distance. In addition, the microstructure images at different cross-sections of the soil column were directly measured by metallographic microscopy, and the particle size distribution characteristics of SPs deposited in quartz sand were measured using a laser particle size analyser. The present study is aimed at investigating the impact of bed filtration of the seepage flow in the presence of widely graded SPs and further reveal the promotion/inhibition mechanism of SPs on the migration of heavy metal contaminants.

2. Experimental Method

2.1. Test Equipment. The main structure of the test equipment consisted of three tempered glass cylinders connected together and containing a test soil sample as a porous medium. Each cylinder had an inner diameter of 8 cm and a height of 30 cm (Figure 1). Rubber O-rings were placed on the flange contact surfaces of the interconnected cylinders and tightly bolted to ensure good water and air tightness of the entire cylinder system. To prevent the soil as the porous medium in the cylinder from being carried away by the seepage flow during the test, a filter screen (the pore size is 0.5 mm) was placed at the seepage outlet (i.e., the bottom of the cylinder system). During the seepage test, a peristaltic pump was employed to continuously inject the prepared solution in the water bath into the soil column at a set seepage velocity. At the seepage outlet, the mixture solution containing SP and heavy metal ions that passed through the soil column was collected for subsequent testing for the relevant concentration and particle gradation data.

The prepared solution was continuously stirred at a set rotational speed using an electric stirrer in a thermostatic water tank (HH-600, Jintan Youlian Instrument Research Institute, Changzhou, China) to avoid precipitation of the added SPs or heavy metal ions. For this purpose, the rotation speed was set to 300 rpm for the small suspended particles (e.g., SPs with a median particle size D_{50} = 227 nm) and 600 rpm for the large

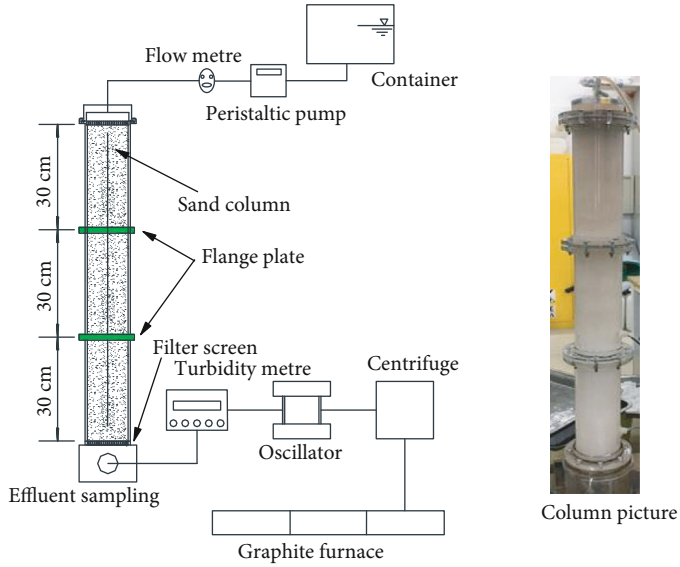

Figure 1: Test apparatus.

ones (e.g., SPs with D_{50} = 13.24 μm). The temperature in the water bath was kept at a constant of (22 ± 0.5°C). A peristaltic pump (Model BT600-2J, Longer Precision Pump, China) was employed to apply a seepage flow, with the actual seepage velocity measured by a flow metre.

The concentration of suspended particles was determined from the turbidity, which was determined using a turbidimeter (Hach2100N, Hach, USA). The mixed solution was shaken using a double-deck shaker (HY-6A, Jintan Zhengrong Experimental Instrument Factory, Changzhou, China) for 8 h at an effective shaking frequency of 100 rpm to allow the added extractant to fully bind with the heavy metal ions to form chelate compounds. The copper ions were separated from the mixture containing SP using a low-speed centrifuge (L3-6K, Kecheng Instrument and Equipment Co., Ltd., Hunan, China) at 4500 rpm for 5 min. The concentration of copper ions in the solution was determined using a graphite furnace atomic absorption spectrophotometer (TAS-990, Beijing Persee General Instrument Co., Ltd, China). The microstructural characteristics of the SPs deposited in the soil columns and quartz sand were determined using an upright metallographic microscope (CX40M, Sunny Optical Technology, Ningbo, China).

2.2. Test Materials. A type of quartz sand was selected as the porous material. Quartz sands were formed by crushing and processing natural quartz, where the main mineral component was SiO_2 (more than 99.9%). The particle density of quartz sand was 2.65 g/cm^3 and was colourless, translucent, and insoluble in acid, with conchoidal fractures and a greasy lustre (Figure 2(a)). Prior to each test, the quartz sand was cleaned with a low concentration of nitric acid solution to remove impurities from its surface and dried at 105°C for 24 h. The particle gradation curve (PGC) of the quartz sand can be seen in Figure 2(a) and shows that particles in the range of 1-2 mm accounted for 22.6% and that those in the range of 2-3.5 mm accounted for 77.4%. The quartz sand had a uniformity coefficient C_u of 1.77, a curvature coefficient C_c of 1.05, and a median diameter D_{50} of 2.2 mm.

The selected SPs were obtained from natural quartz after crushing, ball milling, flotation, purification by acid leaching, and repeated washing with deionized (DI) water. The particle density of SPs was 2.26 g/cm^3 and was mainly composed of SiO_2, with resistance to acid and alkali corrosion. In actual engineering projects, groundwater contains a large number of suspended particles with particle size distribution from a few nm to several mm. When SPs are of transition particle sizes between those of colloids and suspended particles (with a threshold of roughly 1 μm), the particles are affected by a multitude of factors, including hydrodynamic effects, gravity effects, molecular diffusion effects, particle concentration, and electrostatic forces, resulting in a very complex interaction mechanism. Therefore, two sets of widely graded SPs were selected for the present study, which were composed of SPs with different single particle size: one set was white and had particle sizes in the range of 30-2,000 nm with a median particle size D_{50} of 227 nm, and the other set was brownish red and had particle sizes of 2-70 μm with a D_{50} of 13.24 μm. Both sets of SPs contained spherical particles, and their PGCs are shown in Figure 2(b).

Copper ion solutions were prepared using powdered copper nitrate ($Cu(NO_3)_2$) hydrate. The powdered copper nitrate was blue crystals in rhombic flakes and had a relative molecular mass of 187.56, and a stable copper ion solution could be readily prepared by adding water to it. To form stable chelate compounds, ethylenediaminetetraacetic acid (EDTA, $C_{10}H_{16}N_2O_8$) was used as an extractant; this compound can extract heavy metal ions in soil with an efficiency of more than 99% [23, 49, 50]. The disodium salt of ethylenediaminetetraacetic acid (EDTA-2Na, $C_{10}H_{14}N_2Na_2O_8$) could be prepared to improve the solubility of EDTA in water. In the experiment, an extraction solution of 0.05 mol/l was used to maximize the extraction efficiency.

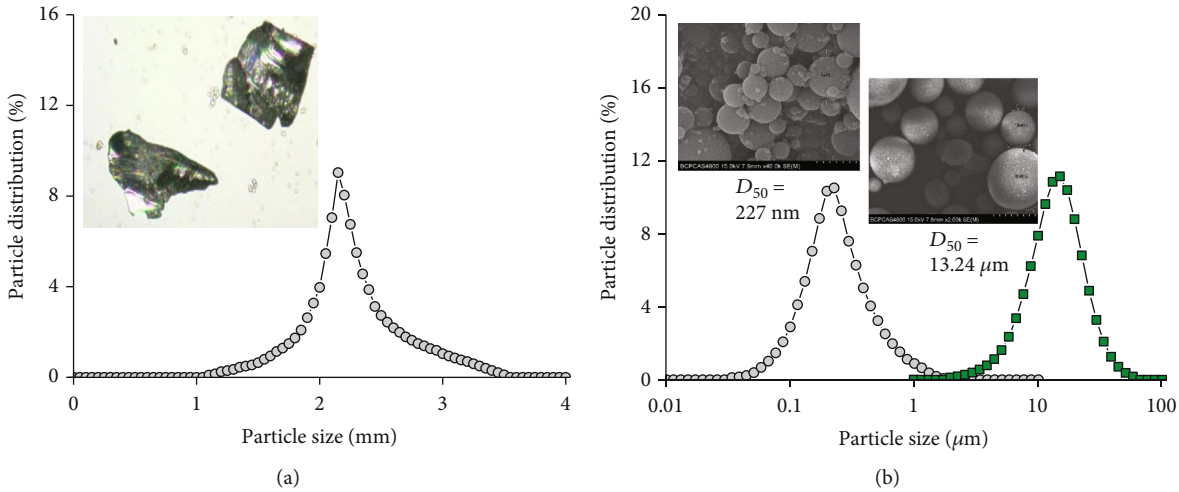

Figure 2: Particle gradation curves of the test materials: (a) quartz sand and (b) silicon powder.

2.3. Test Schemes. The penetration processes of the SPs and copper ions as well as their cotransport in saturated porous media (quartz sand) at room temperature (22°C) and neutral conditions (pH = 7) were studied to investigate the influences of different SP particle concentrations, copper ion concentrations, SP particle size ranges, and seepage velocities on the cotransport process, transport distance, and bed filtration characteristics.

The test cylinders were filled with 10 layers of dried quartz sand, each layer weighing approximately 240 g. Each layer was compacted with a hammer to ensure that the entire experimental sand column eventually had uniform compactness. Before each sand layer was placed, it was necessary to ensure that the surface of DI water was 2 cm above the column surface so that the sand column was fully saturated. The porosity of the experimental column was set to $n = 0.451$. After the entire sand column was in place, the air bubbles on the top of the sand column were removed with DI water, and then the experimental sand column was cleaned with DI water at a seepage velocity of 0.260 cm/s to remove the fine impurities generated during the filling process. The sand column was considered free of impurities when the effluent SP concentration was less than 10^{-4} mg/ml.

The test scheme is shown in Table 1. Three concentrations of SP suspensions and three different concentrations of copper ion solutions were prepared with DI water. During the experiment, an SP suspension, a copper ion solution, or a mixture of the two was injected into the experimental sand column at three different seepage velocities. The Reynolds number of the seepage flow was calculated to be $Re < 116$, which was less than the maximum value of 2300 generally considered for a laminar flow, thereby satisfying the laminar flow condition [28, 38].

For the case where only the SP solution was injected, at regular intervals during the seepage process, the effluent was collected by a small bottle and shaken well, and its turbidity was measured and converted to the corresponding concentration. Similarly, for the case where only the copper ion solution was injected, the absorbance of the copper ion solution in each bottle of the collected effluent was measured and then converted to the copper ion solution concentration based on the relationship between absorbance and concentration. For the case where the SP/copper ion mixture was injected, in addition to the direct measurement of the concentration of SP particles, it was necessary to measure the total concentration of copper ions in the mixture including those adsorbed on the SPs. To this end, a portion of the mixture was poured into a conical flask, and the copper ions attached to the SP particles were detached by EDTA-2Na extraction, shaking, and centrifugation; then, the absorbance of the supernatant was measured and converted to the copper ion concentration. All samples were measured three times in parallel, and the final concentration was taken as the average value.

After a set of seepage tests was completed, approximately 30 g of porous medium particles (i.e., quartz sand, sampled at a thickness of 1 cm) was taken out at each of the different cross-sections of the soil column. The sampling cross-sections were set at the positions of $x = 0$ (i.e., near the injection surface), 30, 60, and 90 cm (i.e., near the effluent plane), and each obtained sample was divided into three parts. For the first part of the sample, extraction, shaking, and centrifugation were performed to determine the deposition/adsorption concentration of copper ions deposited on the quartz sand (including SP). For the second part, the microscopic distribution characteristics of the SP particles and quartz sand were measured by metallographic microscopy. For the third part, the SP deposited on the quartz sand was rinsed with DI water and used to prepare a suspension, and then the PGC of the SP deposited on the quartz sand was obtained using a laser particle size analyser.

3. Test Results

3.1. Influence of the Seepage Velocity. Figure 3 reveals the penetration curves of copper ions during the cotransport of the SPs and copper ions. The horizontal coordinate represents the pore volume (V_P), and the vertical coordinate is the actual concentration of copper ions in the effluent (C, defined as the mass of copper ions in a unit volume of

Table 1: Schemes.

Materials	Median particle size (μm)	SP concentration (mg/ml)	Concentration of copper ions (ng/ml)	Seepage velocity (cm/s)	Number of samples
Copper ions			100, 200, 400	0.087, 0.173, 0.260	$3 \times 3 = 9$
SPs	0.227, 13.24	0.5, 1, 2		0.087, 0.173, 0.260	$2 \times 3 \times 3 = 18$
Copper ions and SPs	0.227, 13.24	0.5, 1, 2	100, 200, 400	0.087, 0.173, 0.260	$3 \times 3 \times 3 \times 3 = 81$

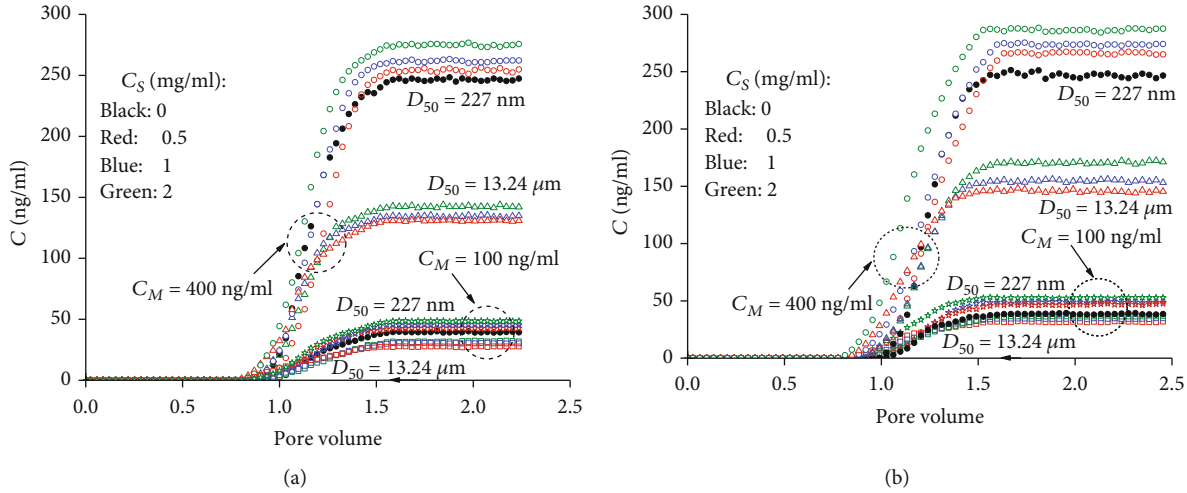

Figure 3: Penetration curves of copper ions at two seepage velocities: (a) $v = 0.087$ cm/s and (b) $v = 0.260$ cm/s.

solution). To enhance the comparability, the ratio of the effluent concentration (C) to the corresponding copper ion injection concentration (C_M) was defined as the relative concentration (C_R), i.e., $C_R = C/C_M$. A comparison of Figures 3(a) and 3(b) indicates that a change in seepage velocity hardly affected the pore volume corresponding to the steady-state concentration of copper ions in the effluent. For example, when the SP solution had an injection concentration C_S of 2 mg/ml and the copper ion solution had an injection concentration C_M of 100 ng/ml, for SP with a size D_{50} of 13.24 μm, the seepage velocities v of 0.087 cm/s, 0.173 cm/s (not shown for lack of space), and 0.260 cm/s corresponded to pore volumes V_P of 1.520, 1.492, and 1.562, respectively (which were very close), for the concentration of copper ions to reach steady state. In comparison, for SP with a D_{50} of 227 nm, the above three seepage velocities corresponded to V_P values of 1.585, 1.492, and 1.526, respectively.

For the case of copper ion injection alone (marked by black symbols in Figure 3), the effluent concentration was almost independent of the seepage velocity (e.g., as shown by a comparison of the data corresponding to the velocities of 0.087 cm/s and 0.173 cm/s). Compared to other heavy metal ions (e.g., Cr^{2+} and Pb^{2+}), copper ions (Cu^{2+}) are very soluble in water and weakly adsorbed to the porous medium matrix [23, 49]; its movement did not differ much from that of the water flow. However, in the presence of the SPs, the concentration of copper ions in the effluent generally slightly increased with increasing seepage velocity. For example, when the SP solution had an injection concentration C_S of 2 mg/ml and the copper ion solution had an injection concentration C_M of 100 ng/ml, for the SP with a median diameter D_{50} of 227 nm, the seepage velocities v of 0.087, 0.173, and 0.260 cm/s led to calculated relative copper ion concentrations C_R of 0.486, 0.518, and 0.526, respectively; in comparison, for SP with a D_{50} of 13.24 μm, the above three seepage velocities corresponded to C_R of 0.274, 0.308, and 0.318, respectively. In fact, there are two transport pathways for copper ions in water. In one pathway, copper ions are dissolved in water and flow through porous media with the injected water flow, and in the other pathway, copper ions are adsorbed on the SPs and migrate out together with the movement of the SPs. There is no significant difference between the two pathways in terms of the number of copper ions dissolved in water and flowing out with water. Regarding the number of copper ions adsorbed on the SPs and migrating out along with them, an increase in the water flow velocity effectively increased the hydrodynamic effect on the SPs and hence reduced the amount of deposited SP. Thereby, this effect accelerated the transport of copper ions due to the close coupling with SP.

3.2. Effect of the SP Size Range. Compared to that in the case of the seepage transport of copper ions alone (i.e., in the absence of SP, marked by black symbols in Figure 3), the concentration of copper ions in the effluent was relatively high in the presence of graded small-scale SP (e.g., $D_{50} = 227$ nm), while it was much lower in the presence of graded large-scale SP. In fact, for graded large-scale SP (e.g., $D_{50} = 13.24$ μm), after a period of continuous injection, a large number

of large SP particles were deposited at the seepage inlet, blocking the seepage channels in the porous medium and in turn significantly retarding the further transport of SP. For graded small-scale SP (e.g., $D_{50} = 227$ nm), the retarding effect caused by seepage in the porous medium was very weak, and in this case, the added SP provided a migration carrier for heavy metal ions, therefore, promoting their migration. For example, when the SP injection concentration C_S was 2 mg/ml, and in the meantime, the copper ion injection concentration C_M was 100 ng/ml, for the graded small-scale SP ($D_{50} = 227$ nm), the seepage velocities v of 0.087, 0.173, and 0.260 cm/s led to relative copper ion concentrations in the effluent C_R of 0.486, 0.518, and 0.526, respectively; for the graded large-scale SP ($D_{50} = 13.24\,\mu$m), the C_R values corresponding to these three seepage velocities were much lower (0.274, 0.308, and 0.318, respectively).

For SPs with different size ranges, the increase in the relative copper ion concentration varied greatly with the seepage velocity. For example, when SP injection concentration C_S was 2 mg/ml and in the meantime the copper ion injection concentration C_M was 100 ng/ml, for graded small-scale SP ($D_{50} = 227$ nm), the relative concentration increased by 12.40% as the seepage velocity v increased from 0.087 cm/s to 0.173 cm/s, while it increased by 3.25% as v increased from 0.173 cm/s further to 0.260 cm/s. For the graded large-scale SP ($D_{50} = 13.24\,\mu$m), the relative concentration increased by 6.58% as the seepage velocity v increased from 0.087 cm/s to 0.173 cm/s, while it increased by 1.54% as v increased from 0.173 cm/s further to 0.260 cm/s. In fact, the graded small-scale SP exists mainly in the form of a suspension in water, so they exert a weak deposition effect owing to the blocking effect but a strong migration ability. Therefore, the increase in the amount of copper ions adsorbed on SP was limited with increasing seepage velocity. However, as the seepage velocity increased, the hydrodynamic effect on graded large-scale SP increased significantly; i.e., the number of copper ions adsorbed on and transported with SPs increased correspondingly.

3.3. Effect of the Injection Concentration of SP. In Figure 4, $C_S = 0$ indicates the case without SP. Since the concentrations of lead ions in the effluent at three water flow velocities were very close, their average values are used here. As the injected SP increased, the copper ion concentration in the effluent increased for the graded small-scale SP (e.g., $D_{50} = 227$ nm); i.e., there was a promoting effect. For example, when the copper ion injection concentration C_M was 100 ng/ml and the seepage velocity v was 0.260 cm/s, the SP injection concentrations C_S of 0, 0.5, 1, and 2 mg/ml led to relative concentrations of copper ions in the effluent C_R of 0.385, 0.468, 0.487, and 0.526, respectively; in comparison, for the graded large-scale SP ($D_{50} = 13.24\,\mu$m), the concentrations of copper ions in the effluent decreased with increasing SP injection concentration. That is, the SP injection concentrations C_S of 0, 0.5, 1, and 2 mg/ml corresponded to relative concentrations of copper ions in the effluent C_R of 0.385, 0.366, 0.344, and 0.318, respectively. An increase of the injected SP brought about an increase in the number of copper ions adsorbed on the SP. However, an increase in the SP injection concentration had a strong promoting effect on the copper ions with the graded small-scale SP due to their weak deposition effect and a strong inhibiting effect on copper ions in the case of graded large-scale SP due to their strong deposition effect.

In addition, the relative concentrations of copper ions in the effluent in the presence of SPs with the two different size ranges increased, albeit to different extents, with increasing copper ion injection concentration. In other words, the increase in the relative copper ion concentration (C_R) with the graded small-scale SP ($D_{50} = 227$ nm) was significantly larger than that with the graded large-scale SP ($D_{50} = 13.24\,\mu$m). For example, when C_S was 0.5 mg/ml, as the copper ion injection concentration C_M increased from 100 ng/ml (Figure 4(a)) to 400 ng/ml (Figure 4(b)), the increase in the relative copper ion concentration with the graded small-scale SP ($D_{50} = 227$ nm) was 45.4% (i.e., $C_R = 0.449 \rightarrow 0.653$, the average value at the three different seepage velocities), while that with the graded large-scale SP ($D_{50} = 13.24\,\mu$m) was 13.8% (i.e., $C_R = 0.347 \rightarrow 0.395$, the average value at the three different seepage velocities).

4. Discussion

4.1. Deposition of Copper Ions along the Transport Distance. Figure 5 shows that the deposition concentration of copper ions at the cross-section of the soil column (σ_M, determined as the ratio of the deposited copper ions to porous materials in mass per unit volume) attenuated as the transport distance increased. The deposition concentration distribution of copper ions migrating alone in the soil column is also given in Figure 5 (marked by black symbols). Since the test results at the three water flow velocities were very close, their average values are used here. In the presence of graded small-scale SP ($D_{50} = 227$ nm), the decrease in the deposition concentration of copper ions was relatively gentle in the range of transport distance $x = 0 - 90$ cm. In this case, the main reason for deposition during the transport process was adsorption by the porous medium matrix. As the transport distance of the SP increased, the heavy metal ions adsorbed on the surface of SP decreased, eventually resulting in a relatively gentle decrease in the deposition of copper ions with increasing transport distance.

For graded large-scale SP ($D_{50} = 13.24\,\mu$m), the deposition concentration of copper ions decreased very steeply over a transport distance x of 0 to 30 cm, but the decrease began to level off over a longer transport distance x of 30 to 90 cm and roughly coincided with the conditions in the presence of graded small-scale SP. In fact, with the graded large-scale SP (e.g., $D_{50} = 13.24\,\mu$m), the porous medium had an apparent retarding influence on the relatively large SP particles from the very beginning due to bed filtration. Under this condition, the deposition process was mainly concentrated in a small region away from the injection inlet, and only SP with particle sizes smaller than a certain scale could continue to migrate farther away. Eventually, most of the copper ions adsorbed on the large SP particles were deposited in this region, thus, resulting in a high deposition concentration of copper ions there. Thereafter, as the transport distance

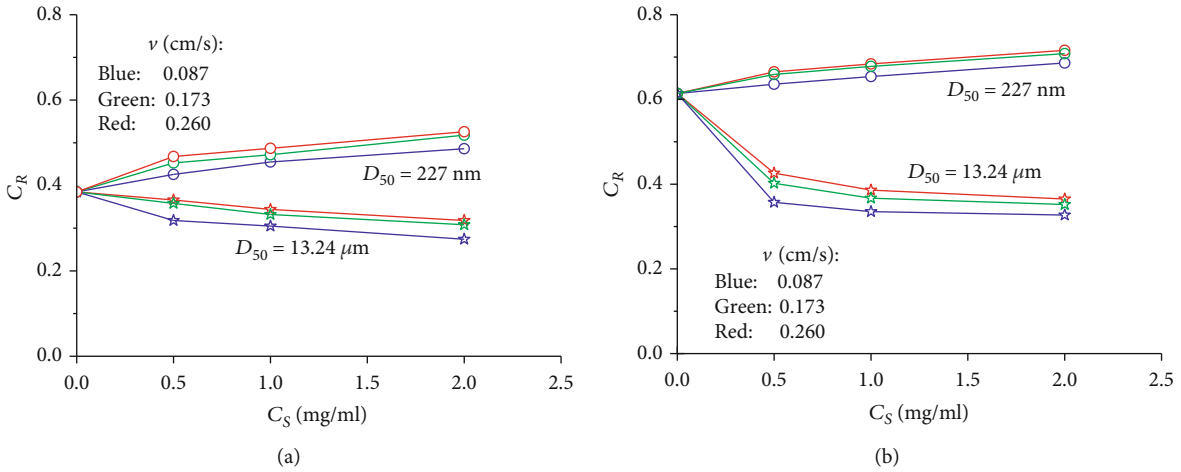

Figure 4: Relative density of copper ions with increasing SP injection concentration: (a) C_M = 100 ng/ml and (b) C_M = 400 ng/ml.

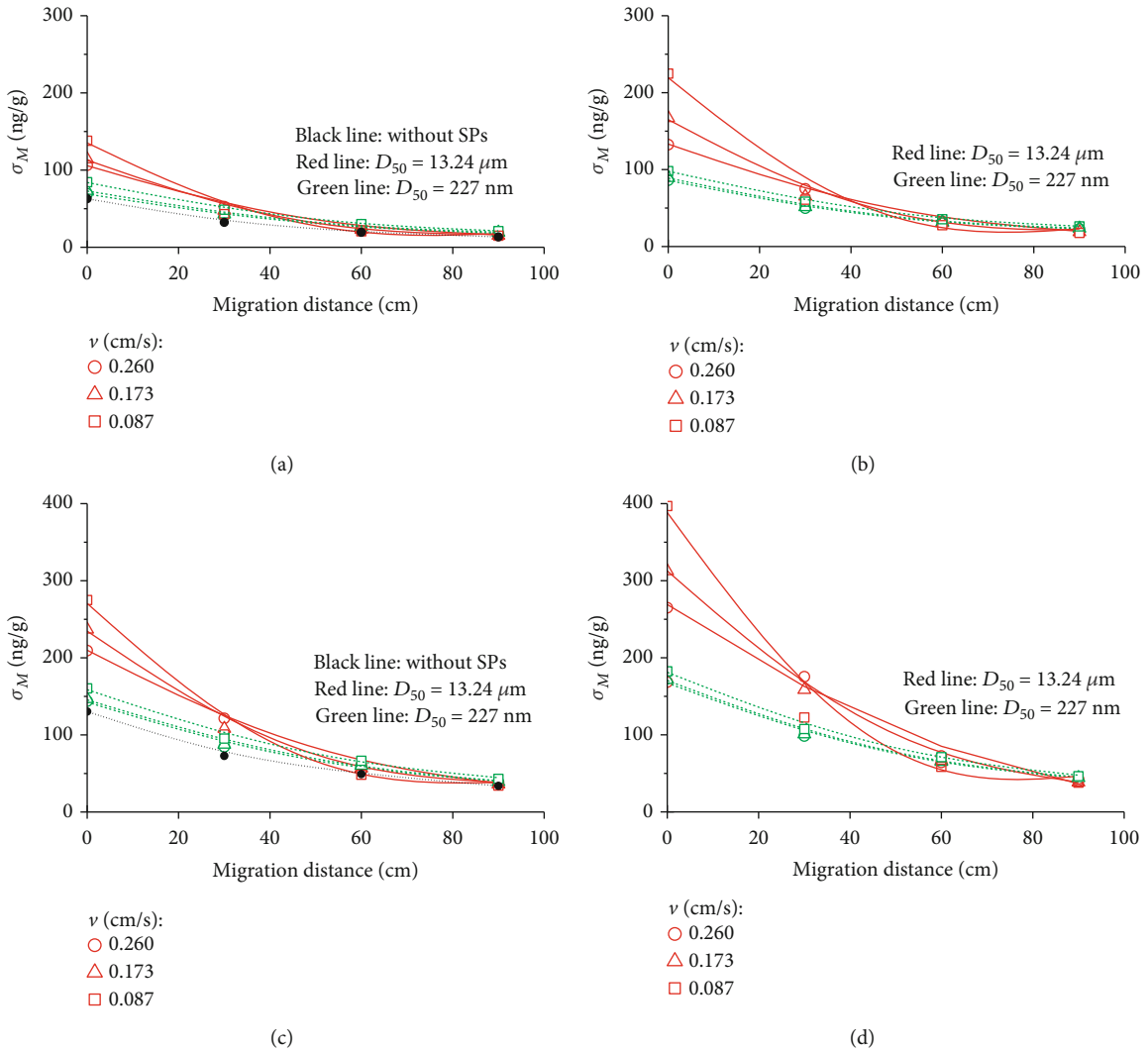

Figure 5: The deposition concentrations of copper ions along the transport distance: (a) C_M = 100 ng/ml, C_S = 0.5 mg/ml; (b) C_M = 100 ng/ml , C_S = 2 mg/ml; (c) C_M = 400 ng/ml, C_S = 0.5 mg/ml; and (d) C_M = 400 ng/ml, C_S = 2 mg/ml.

further increased, the deposition process of the fine SP after the early filtration stage became gentle, and the reduction in the number of copper ions adsorbed on the SP decreased accordingly. Certainly, the portion of copper ions dissolved in and moving with the water was hardly affected.

Compared with the case without SP (marked by black symbols in Figure 5), the addition of SP increased the deposition concentration of copper ions at each cross-section. When the seepage velocity v was 0.260 cm/s and in the meantime the copper ion injection concentration C_M was 400 ng/ml, the SP injection concentrations C_S of 0, 0.5, 1, and 2 mg/ml corresponded to copper ion deposition concentrations of 75.48, 84.57, 90.72, and 98.46 ng/g, respectively, for the graded small-scale SP ($D_{50} = 227$ nm) and 75.48, 121.36, 144.87, and 175.41 ng/g, respectively, for the graded large-scale SP ($D_{50} = 13.24\,\mu$m) at a transport distance x of 30 cm. The results indicate that the more the injected SP was, the higher the SP deposition concentration at each cross-section and the larger the number of deposited copper ions in the presence of large-scale SP. In the presence of small-scale SP, since the number of deposited copper ions closer to the injection inlet was relatively small, their transport distances were extended (i.e., the promoting effect). However, after a relatively long transport distance, the presence of SP still had an overall retarding effect on copper ions. The so-called "size exclusion effect" was evident only in the relatively large pore channels inside the porous medium.

Certainly, as the copper ion injection concentration increased, the concentration of copper ions deposited at each cross-section increased. For example, when the copper ion concentration C_M changed from 100 to 400 ng/ml (compare Figures 5(a) and 5(c) or Figures 5(b) and 5(d)), the deposition concentration of copper ions increased significantly.

In addition, with increasing transport distance ($x = 0$, 30, 60, and 90 cm), the SP deposition concentration decreased as the seepage velocity increased. The hydrodynamic effect on SP particles increased at a high seepage velocity, promoting the SP particles to migrate farther away. A comparison of the data corresponding to two velocities ($v = 0.087$ and 0.260 cm/s) in Figure 5(a) clearly states that in the presence of graded large-scale SP, an increase of the water flow velocity brought about an increase in the copper ion deposition concentration farther from the injection inlet and a decrease, to some extent, in that closer to the injection inlet.

4.2. PGCs of SPs at Different Column Cross-Sections. Figure 6 shows the PGCs of the injected SPs and the evolution of the PGCs of the SPs at four different transport distances at two seepage velocities. In fact, the deposition of SPs during the seepage transport process includes the attachment to the porous medium matrix (i.e., the adsorption effect) and the embedding in the small pores of the porous media (i.e., the blocking effect). For graded small-scale SP (Figures 6(a) and 6(b), $D_{50} = 227$ nm), the deposition owing to the adsorption action of the matrix was relatively high, and the blocking due to the scale effect of the SP particles was very low. Therefore, the PGCs of the SP particles deposited at different cross-sections of the soil column in the seepage process at the same seepage velocity almost coincided. For example, under the conditions where the SP injection concentration C_S was 2 mg/ml and the copper ion injection concentration C_M was 400 ng/ml, as the water flow velocity v was 0.087 cm/s (Figure 6(a)), the median particle sizes D_{50} of the SP deposited at transport distances x of 0, 30, 60, and 90 cm were 218.93, 206.39, 206.65, and 223.56 nm, respectively, which differ minimally (with an average $D_{50} = 213.88$ nm) and differ minimally from the particle sizes of the injected SP (i.e., $D_{50} = 227$ nm). In addition, since the small-scale SP particles were subjected to weak hydrodynamic effects, the median particle size of the SP at each transport distance increased slightly (with a mean value of $D_{50} = 227.16$ nm) as the water flow velocity increased (e.g., to 0.260 cm/s; Figure 6(b)). That is, the copper ions adsorbed on the surface of and carried by the SP were deposited gradually with the deposition of SP without any significant changes with changing seepage velocity.

The small pores in the porous media had an enhanced embedding effect on the graded large-scale SP (Figures 6(c) and 6(d), $D_{50} = 13.24\,\mu$m). That is, the bed filtration of the seepage flow was significantly enhanced, resulting in a notable increase in the size of the SP deposited on the injection inlet ($x = 0$, marked by red symbols) compared to that of the injected SP. As the transport distance increased, the median particle size of the SP deposited on other cross-sections gradually decreased. As the water flow velocity v was 0.087 cm/s, the median particle sizes D_{50} of the SP deposited at transport distances x of 0, 30, 60, and 90 cm were 27.38, 7.64, 4.23, and 3.31 μm, respectively (Figure 6(c)), meaning that the SP particles deposited at a relatively long distance were smaller than the injected SP particles. In addition, as the seepage velocity increased (e.g., from 0.087 to 0.260 cm/s, Figure 6(d)), the median particle size D_{50} of the deposited SP decreased (i.e., 22.06 μm) at the transport distance $x = 0$ and at longer transport distances ($x = 30$, 60, and 90 cm) increased (10.44, 7.27, and 4.80 μm, respectively). In fact, in this situation, the hydrodynamic effect on the SP particles was significantly enhanced, so more large SP particles passed through the pore channels of the porous media and advanced to a distant position but were eventually gradually deposited as the transport distance increased. This phenomenon indicates that bed filtration has a remarkable action on the deposition process of large SP particles [23, 47, 51], which should be considered when dealing with the transport of widely graded SPs in practical engineering projects. In other words, the number of copper ions adsorbed on the graded large-scale SP was limited compared to that on the graded small-scale SP, while most of the copper ions were present in water-soluble form. However, the bed filtration of the graded large-scale SP was significant, i.e., most of the SP particles were deposited within a limited distance from the injection inlet ($x = 0$ to 30 cm). Therefore, there was an overall retarding effect on copper ions. This agrees with the results of the penetration curves for copper ions given in Figure 3.

4.3. Microscopic Images at Different Column Cross-Sections. Figure 7 shows the typical microstructural characteristics of quartz sand at different cross-sections of the soil column and

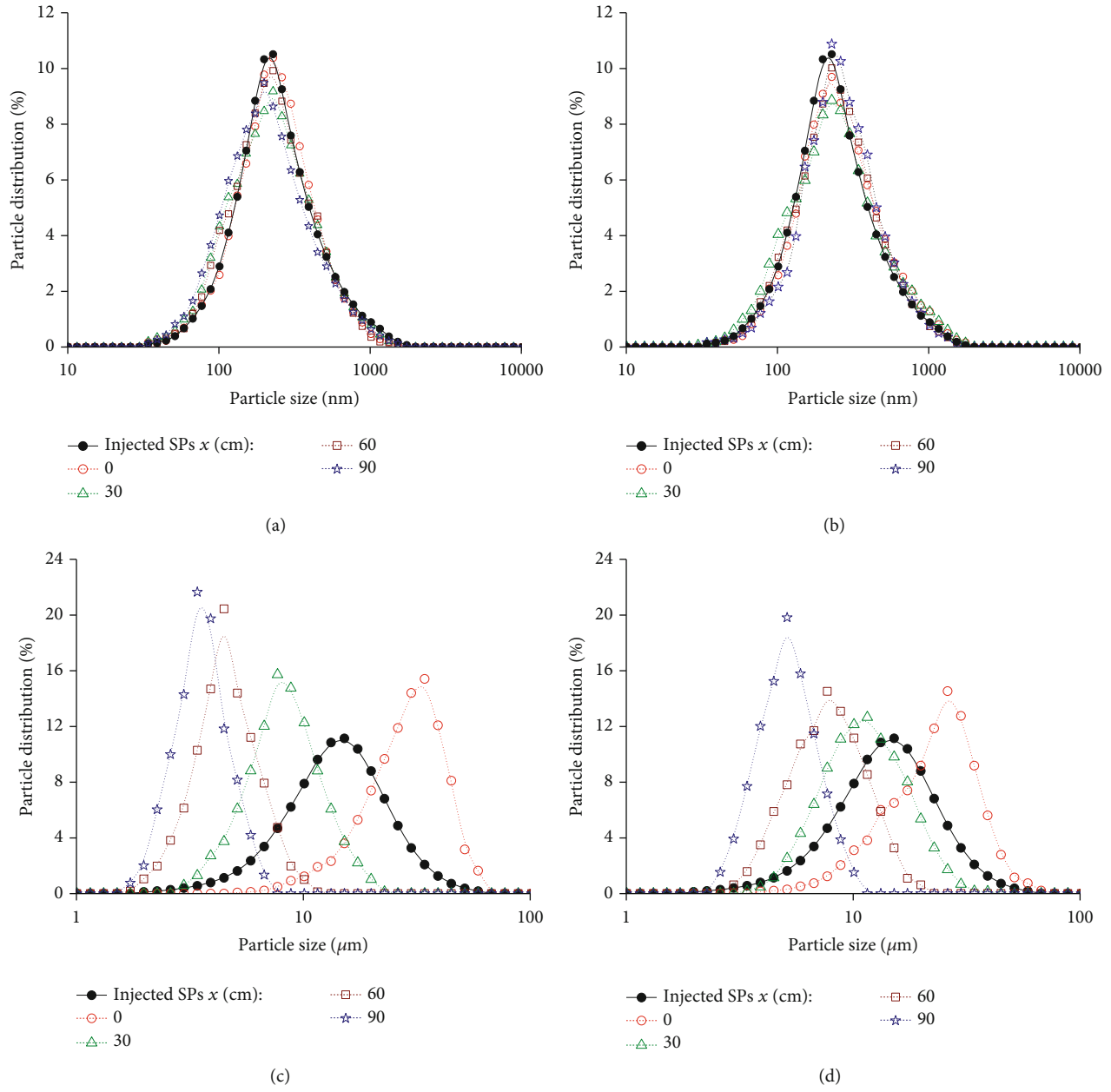

FIGURE 6: Particle gradation curves of the SPs: (a) $v = 0.087$ cm/s, $D_{50} = 227$ nm; (b) $v = 0.260$ cm/s, $D_{50} = 227$ nm; (c) $v = 0.087$ cm/s, $D_{50} = 13.24\,\mu$m; and (d) $v = 0.087$ cm/s, $D_{50} = 13.24\,\mu$m.

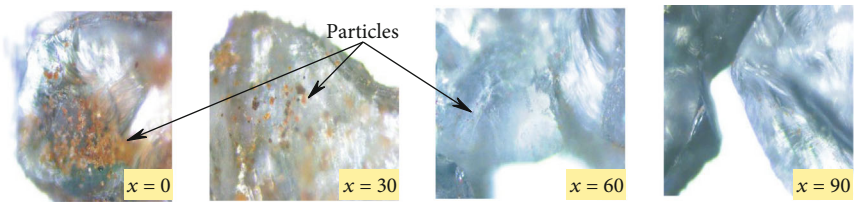

FIGURE 7: Microscope images at different column cross-sections x (unit: cm).

the SP deposited on those cross-sections (as brownish-red particles) for the conditions of $D_{50} = 13.24\,\mu$m and $C_M = 400$ ng /ml obtained using metallographic microscopy. In Figure 7, the water flow velocity is $v = 0.260$ cm/s, and SP injection concentration is $C_S = 0.5$ mg/ml. The number of SP particles attached to the quartz sand decreased significantly with increasing transport distance ($x = 0 \rightarrow 30 \rightarrow 60 \rightarrow 90$ cm). Test results also show that, as the SP injection concentration

increased, the number of SP retained in the sand increased. At the transport distance x of 90 cm, the number of SP retained in the sand was already very small under each SP injection concentration, and the corresponding transport distance of the SP was limited to a small range. That is, after a long penetration distance, the copper ions in the effluent mainly existed in a free, water-soluble form. Therefore, the presence of large SP particles actually retarded the transport of heavy metal pollutants.

Microscope images reveal that, as the seepage velocity increased, the transport distance of the SPs increased significantly, consistent with the evolution of the PGCs shown in Figures 6(c) and 6(d). The strong electrostatic interaction between oppositely charged heavy metals and SPs with negative charges is of great significance. As mentioned earlier, the deposition of the SPs in the transport process is mainly reflected in two aspects. First, the positively charged copper ions are adsorbed on the SP particles, and then an electrostatic attraction is generated between the copper ions and the porous medium matrix with a negatively charged surface, eventually causing a portion of the SP to be deposited onto the matrix surface. Second, the SPs are embedded in the pores in the process of continuous collision with its pore channels, a process that advances with the enhancement of the hydrodynamic effect.

5. Conclusion

The paper reveals the promotion/inhibition mechanism of SPs on the migration of heavy metal contaminants. The presence of graded large-scale silicon powder (SP) clearly has an inhibiting effect on the transport of copper ions in the seepage transport process. In contrast, the presence of graded small-scale SP can even bring about an increase in the effluent concentration of copper ions, exhibiting a certain promoting effect. That is, the transport distance of copper ions under the presence of graded small-scale SP is greater than that under the presence of graded large-scale SP. However, with a long transport distance, the presence of SPs, regardless of particle sizes, has an overall retarding effect on copper ions.

In general, the concentration of copper ions in the effluent increases with increasing seepage velocity, but the pore volume corresponding to the steady-state concentration is approximately constant. In addition, the promoting effect of an increase in seepage velocity on copper ions is much greater under the presence of graded large-scale SP than under the presence of graded small-scale SP; as the seepage velocity increases, the deposition concentration of copper ions far from the injection plane tends to increase.

From the perspective of microstructural characteristics, the average particle size of the SP deposited at different transport distances for graded small-scale SP is almost constant, whereas the average particle size of graded large-scale SP shows a significant decrease with increasing transport distance, demonstrating notable bed filtration. This also determines the sequence and rate of the retarding effect of SPs on heavy metal ions under seepage flow.

Data Availability

The research article data used to support the findings of this study are available from the corresponding author upon request.

Additional Points

Highlights. (1) After a long transport distance, the presence of SPs, regardless of particle size, has an overall retarding effect on the transport of Cu^{2+}. (2) The effect of the increase in seepage velocity on the effluent concentration of Cu^{2+} is greater with the graded large-scale than with the graded small-scale SPs. (3) The deposition of SPs is directly imaged by metallographic microscopy, which demonstrates a notable bed filtration effect.

Conflicts of Interest

The authors declare that they have no conflicts of interest.

Acknowledgments

The authors are grateful to the National Natural Science Foundation of China (52079003 and 52078031).

References

[1] Z. Lin, Y. Hu, Y. Yuan, B. Hu, and B. Wang, "Comparative analysis of kinetics and mechanisms for Pb(II) sorption onto three kinds of microplastics," *Ecotoxicology and Environmental Safety*, vol. 208, p. 111451, 2021.

[2] B. Wang, Y. Li, J. Zheng, Y. Hu, X. Wang, and B. Hu, "Efficient removal of U(VI) from aqueous solutions using the magnetic biochar derived from the biomass of a bloom-forming cyanobacterium (*Microcystis aeruginosa*)," *Chemosphere*, vol. 254, p. 126898, 2020.

[3] S. Li, L. Dong, Z. Wei, G. Sheng, K. Du, and B. Hu, "Adsorption and mechanistic study of the invasive plant-derived biochar functionalized with CaAl-LDH for Eu(III) in water," *Journal of Environmental Sciences*, vol. 96, pp. 127–137, 2020.

[4] G. Yang, "Thermo-hydro-mechanical model for unsaturated clay soils based on granular solid hydrodynamics theory," *International Journal of Geomechanics*, vol. 19, no. 10, article 04019115, 2019.

[5] X. Z. Cui, Y. Fan, H. Wang, and S. Huang, "Ground environment characteristics during the operation of GWHP considering the particle deposition effect," *Energy and Buildings*, vol. 206, article 109593, 2020.

[6] B. Bai, J. Q. Wang, Z. Q. Zhai, and T. Xu, "The penetration processes of red mud filtrate in a porous medium by seepage," *Transport in Porous Media*, vol. 117, no. 2, pp. 207–227, 2017.

[7] X. Z. Cui, Y. Fan, H. X. Wang, and S. Huang, "Experimental investigation of suspended particles transport in porous medium under variable temperatures," *Hydrological Processes*, vol. 33, no. 7, pp. 1117–1126, 2019.

[8] B. Bai and X. Shi, "Experimental study on the consolidation of saturated silty clay subjected to cyclic thermal loading," *Geomechanics and Engineering*, vol. 12, no. 4, pp. 707–721, 2017.

[9] S. Lee, I. W. Ko, I. H. Yoon, D. W. Kim, and K. W. Kim, "Colloid mobilization and heavy metal transport in the sampling of

soil solution from Duckum soil in South Korea," *Environmental Geochemistry and Health*, vol. 41, no. 1, pp. 469–480, 2019.

[10] B. Hudcova, V. Veselska, J. Filip, S. Cihalova, and M. Komarek, "Highly effective Zn(II) and Pb(II) removal from aqueous solutions using Mg-Fe layered double hydroxides: comprehensive adsorption modeling coupled with solid state analyses," *Journal of Cleaner Production*, vol. 171, pp. 944–953, 2018.

[11] B. Bai, S. C. Jiang, L. L. Liu, X. Li, and H. Y. Wu, "The transport of silica powders and lead ions under unsteady flow and variable injection concentrations," *Powder Technology*, vol. 387, pp. 22–30, 2021.

[12] S. Raikova, M. Piccini, M. K. Surman, M. J. Allen, and C. J. Chuck, "Making light work of heavy metal contamination: the potential for coupling bioremediation with bioenergy production," *Journal of Chemical Technology and Biotechnology*, vol. 94, no. 10, pp. 3064–3072, 2019.

[13] X. Cui, Q. Liu, C. Zhang, Y. Huang, Y. Fan, and H. Wang, "Land subsidence due to groundwater pumping and recharge: considering the particle-deposition effect in ground-source heat-pump engineering," *Hydrogeology Journal*, vol. 26, no. 3, pp. 789–802, 2018.

[14] D. Rao and B. Bai, "Study of the factors influencing diffusive tortuosity based on pore-scale SPH simulation of granular soil," *Transport in Porous Media*, vol. 132, no. 2, pp. 333–353, 2020.

[15] X. Chen and B. Bai, "Experimental investigation and modeling of particulate transportation and deposition in vertical and horizontal flows," *Hydrogeology Journal*, vol. 23, no. 2, pp. 365–375, 2015.

[16] G. E. Walshe, L. P. Pang, M. Flury, M. E. Close, and M. Flintoft, "Effects of pH, ionic strength, dissolved organic matter, and flow rate on the co-transport of MS2 bacteriophages with kaolinite in gravel aquifer media," *Water Research*, vol. 44, no. 4, pp. 1255–1269, 2010.

[17] B. Bai, G. C. Yang, T. Li, and G. S. Yang, "A thermodynamic constitutive model with temperature effect based on particle rearrangement for geomaterials," *Mechanics of Materials*, vol. 139, p. 103180, 2019.

[18] Z. L. Li and L. X. Zhou, "Cadmium transport mediated by soil colloid and dissolved organic matter: a field study," *Journal of Environmental Sciences*, vol. 22, no. 1, pp. 106–115, 2010.

[19] N. Natarajan and G. S. Kumar, "Spatial moment analysis of colloid facilitated radionuclide transport in a coupled fracture-matrix system," *International Journal of Energy and Environment*, vol. 2, no. 3, pp. 491–504, 2011.

[20] V. Nikonov, V. Goryainova, and N. Lukina, "Ni and Cu migration and accumulation in forest ecosystems on the Kola Peninsula," *Chemosphere*, vol. 42, no. 1, pp. 93–100, 2001.

[21] B. Bai, T. Xu, and Z. Guo, "An experimental and theoretical study of the seepage migration of suspended particles with different sizes," *Hydrogeology Journal*, vol. 24, no. 8, pp. 2063–2078, 2016.

[22] J. Kumpiene, A. Lagerkvist, and C. Maurice, "Stabilization of As, Cr, Cu, Pb and Zn in soil using amendments - a review," *Waste Management*, vol. 28, no. 1, pp. 215–225, 2008.

[23] B. Bai, Q. Nie, Y. Zhang, X. Wang, and W. Hu, "Cotransport of heavy metals and SiO_2 particles at different temperatures by seepage," *Journal of Hydrology*, vol. 597, p. 125771, 2021.

[24] X. Z. Cui, Q. S. Liu, and C. Y. Zhang, "Detachment characteristics of deposited particles in porous medium: experimentation and modeling," *Transport in Porous Media*, vol. 119, no. 3, pp. 633–647, 2017.

[25] Q. Feng, L. Cha, C. Dai, G. Zhao, and S. Wang, "Effect of particle size and concentration on the migration behavior in porous media by coupling computational fluid dynamics and discrete element method," *Powder Technology*, vol. 360, pp. 704–714, 2020.

[26] C. Huang, C. Tong, W. Hu, H. Yeh, and T. Yang, "Analysis of radially convergent tracer test in a two-zone confined aquifer with vertical dispersion effect: asymmetrical and symmetrical transports," *Journal of Hazardous Materials*, vol. 377, pp. 8–16, 2019.

[27] H. Zhang, G. V. C. Malgaresi, and P. Bedrikovetsky, "Exact solutions for suspension-colloidal transport with multiple capture mechanisms," *International Journal of Non-Linear Mechanics*, vol. 105, pp. 27–42, 2018.

[28] B. Bai, F. Long, D. Y. Rao, and T. Xu, "The effect of temperature on the seepage transport of suspended particles in a porous medium," *Hydrological Processes*, vol. 31, no. 2, pp. 382–393, 2017.

[29] B. Bai, L. Guo, and S. Han, "Pore pressure and consolidation of saturated silty clay induced by progressively heating/cooling," *Mechanics of Materials*, vol. 75, pp. 84–94, 2014.

[30] C. V. Chrysikopoulos and V. I. Syngouna, "Effect of gravity on colloid transport through water-saturated columns packed with glass beads: modeling and experiments," *Environmental Science and Technology*, vol. 48, no. 12, pp. 6805–6813, 2014.

[31] V. I. Syngouna and C. V. Chrysikopoulos, "Cotransport of clay colloids and viruses through water-saturated vertically oriented columns packed with glass beads: gravity effects," *Science of the Total Environment*, vol. 545–546, pp. 210–218, 2016.

[32] B. Bai, Y. Ren, and D. Rao, "The transport of solid particle suspension at different alkalinities in saturated porous media," *Journal of Porous Media*, vol. 23, no. 3, pp. 207–218, 2020.

[33] S. Nishad and R. I. Al-Raoush, "Colloid retention and mobilization mechanisms under different physicochemical conditions in porous media: a micromodel study," *Powder Technology*, vol. 377, pp. 163–173, 2021.

[34] C. V. Chrysikopoulos, N. P. Sotirelis, and N. G. Kallithrakas-Kontos, "Cotransport of graphene oxide nanoparticles and kaolinite colloids in porous media," *Transport in Porous Media*, vol. 119, no. 1, pp. 181–204, 2017.

[35] B. Bai, Z. Zhai, and D. Rao, "The seepage transport of heavy metal Pb^{2+} through sand column in the presence of silicon powders," *Journal of Hydrology and Hydromechanics*, vol. 67, no. 4, pp. 349–358, 2019.

[36] B. Bai, "Fluctuation responses of saturated porous media subjected to cyclic thermal loading," *Computers and Geotechnics*, vol. 33, no. 8, pp. 396–403, 2006.

[37] T. Russell and P. Bedrikovetsky, "Colloidal-suspension flows with delayed fines detachment: analytical model & laboratory study," *Chemical Engineering Science*, vol. 190, pp. 98–109, 2018.

[38] C. V. Chrysikopoulos and V. E. Katzourakis, "Colloid particle size-dependent dispersivity," *Water Resources Research*, vol. 51, no. 6, pp. 4668–4683, 2015.

[39] P. Bedrichovskysky, Z. You, A. Badalyan, Y. Osipov, and L. Kuzmina, "Analytical model for straining-dominant large-retention depth filtration," *Chemical Engineering Journal*, vol. 330, pp. 1148–1159, 2017.

[40] S. Borazjani and P. Bedrikovetsky, "Exact solutions for two-phase colloidal-suspension transport in porous media," *Applied Mathematical Modelling*, vol. 44, pp. 296–320, 2017.

[41] V. E. Katzourakis and C. V. Chrysikopoulos, "Two-site colloid transport with reversible and irreversible attachment: analytical solutions," *Advances in Water Resources*, vol. 130, pp. 29–36, 2019.

[42] B. Bai, D. Y. Rao, T. Chang, and Z. G. Guo, "A nonlinear attachment-detachment model with adsorption hysteresis for suspension-colloidal transport in porous media," *Journal of Hydrology*, vol. 578, p. 124080, 2019.

[43] P. Bedrikovetsky, A. Zeinijahromi, F. D. Siqueira, C. A. Furtado, and A. L. S. de Souza, "Particle detachment under velocity alternation during suspension transport in porous media," *Transport in Porous Media*, vol. 91, no. 1, pp. 173–197, 2012.

[44] B. Bai, D. Y. Rao, T. Xu, and P. P. Chen, "SPH-FDM boundary for the analysis of thermal process in homogeneous media with a discontinuous interface," *International Journal of Heat and Mass Transfer*, vol. 117, pp. 517–526, 2018.

[45] X. Y. Tang and N. Weisbrod, "Colloid-facilitated transport of lead in natural discrete fractures," *Environmental Pollution*, vol. 157, no. 8-9, pp. 2266–2274, 2009.

[46] S. Sasidharan, S. Torkzaban, A. Scott, B. P. J. Dillon, and P. G. Cook, "Coupled effects of hydrodynamic and solution chemistry on long-term nanoparticle transport and deposition in saturated porous media," *Colloids and Surfaces A: Physicochemical and Engineering Aspects*, vol. 457, pp. 169–179, 2014.

[47] Y. Sun, B. Gao, S. A. Bradford et al., "Transport, retention, and size perturbation of graphene oxide in saturated porous media: effects of input concentration and grain size," *Water Research*, vol. 68, pp. 24–33, 2015.

[48] T. Ikni, A. Bennamar, M. Kadri, N. D. Ahfir, and H. Q. Wang, "Particle transport within water-saturated porous media: effect of pore size on retention kinetics and size selection," *Comptes Rendus Geoscience*, vol. 345, no. 9-10, pp. 392–400, 2013.

[49] B. Bai, J. Zhang, L. Liu, and Y. Ji, "The deposition characteristics of coupled lead ions and suspended silicon powders along the migration distance in water seepage," *Transport in Porous Media*, vol. 134, no. 3, pp. 707–724, 2020.

[50] J. Qiao, H. Sun, X. Luo, W. Zhang, S. Mathews, and X. Yin, "EDTA-assisted leaching of Pb and Cd from contaminated soil," *Chemosphere*, vol. 167, pp. 422–428, 2017.

[51] L. Chequer, P. Bedrikovetsky, A. Badalyan, and V. Gitis, "Water level and mobilisation of colloids in porous media," *Advances in Water Resources*, vol. 143, p. 103670, 2020.